International Journal of Nanomedicine

Dovepress
open access to scientific and medical research

Open Access Full Text Article

ORIGINAL RESEARCH

Biomimetic Copper-Doped Polypyrrole Nanoparticles for Enhanced Cancer Low-Temperature Photothermal Therapy

Hao Chen[1,*], Xi Luo[1,*], Wei Cai[2,*], Shile Wang[3], Jingfeng Xiang[1], Zeming Liu[4], Daoming Zhu[1,5]

[1]Department of General Surgery & Guangdong Provincial Key Laboratory of Precision Medicine for Gastrointestinal Tumor, Nanfang Hospital, The First School of Clinical Medicine, Southern Medical University, Guangzhou, Guangdong, 510515, People's Republic of China; [2]Department of Radiology, Tongji Hospital, Tongji Medical College, Huazhong University of Science and Technology, Wuhan, 430030, People's Republic of China; [3]Academy of Medical Sciences, The Second Affiliated Hospital of Zhengzhou University, Zhengzhou University, Zhengzhou, 450052, People's Republic of China; [4]Department of Plastic Surgery, Tongji Hospital, Tongji Medical College, Huazhong University of Science and Technology, Wuhan, 430030, People's Republic of China; [5]Department of Electronic Science and Technology, School of Physics and Technology, Wuhan University, Wuhan, 430072, People's Republic of China

*These authors contributed equally to this work

Correspondence: Zeming Liu; Daoming Zhu, Email zemingliutj@163.com; zhudaoming666@smu.edu.cn

Introduction: Photothermal therapy (PTT) has a significant potential for its application in precision tumour therapy. However, PTT-induced hyperthermia may damage healthy tissues and trigger the expression of heat shock proteins (HSPs), thereby compromising the long-term therapeutic efficacy of PTT.

Methods: In this study, a biomimetic drug delivery system comprising CuP nanozymes as the inner core and platelet membrane (PM) as the outer shell was successfully developed for administering synergistic chemodynamic therapy and mild PTT. PM is encapsulated on CuP to form this biomimetic nanoparticle (PM-coated CuP nanoparticles, PC). PC possesses peroxidase (POD) activity, can facilitate the conversion of hydrogen peroxide into ·OH, thereby inhibiting the expression of HSPs.

Results: Upon exposure to low-power laser irradiation (0.5 W/cm^2, 1064 nm), PC can convert near-infrared II laser energy into heat energy, thereby enabling the administration of enhanced mild PTT. In vitro and in vivo experiments have demonstrated that this synergistic approach can induce over 90% tumour eradication with favourable biocompatibility.

Discussion: PC exhibits high efficacy and biocompatibility, making it a promising candidate for future applications.

Keywords: biomimetic nanoparticles, copper-doped polypyrrole nanoparticles, low-temperature photothermal therapy

Introduction

Photothermal therapy (PTT) is a method to treat cancers using near-infrared light (NIR).[1,2] PTT kills tumour cell by converting the absorbed light energy into heat energy upon the irradiation of the photothermal agent (PTA) with a near-infrared laser to ablate the tumour.[3–5] PTT has great potential for clinical application owing to its several advantages, including its non-invasive nature, few adverse reactions and low systemic toxicity, and it has become a highly popular cancer treatment method.[6,7] For complete tumour ablation, high-temperature PTT (>50°C) is often used to induce complete cell necrosis.[8] However, hyperthermia and high-intensity laser irradiation associated with this approach inevitably damage nearby healthy tissues.[9] In addition, PTT can activate the heat shock response, which exerts cell-protective and anti-apoptotic effects, and induce the overexpression of heat shock proteins (HSPs).[10] HSPs participate in the development of instantaneous heat resistance and acquisition of permanent heat resistance, thereby enhancing the heat resistance of tumour cells and helping them to resist PTT.[9] HSP 90 and HSP 70 proteins, which belong to the HSPs family, can help cancer cells fight against harsh environment, repair cell damage caused by photothermal therapy and improve their survival.[11]

Received: 30 June 2023
Accepted: 5 December 2023
Published: 12 December 2023

As messengers of cell injury, reactive oxygen species (ROS) can cause extensive cell damage by oxidising cell membranes and destroying proteins and DNA.[12–26] Excessive ROS production is associated with many forms of apoptosis and necrosis.[15,17,19,20,27,28] Studies have confirmed a correlation between ROS production and HSPs induced expression.[11] HSP 70 plays a similar role to small molecular heat shock protein in the process of resisting oxidative stress. And HSP 90 in mouse tissues and cells can resist heat-induced apoptosis by inhibiting ROS induction.[29] Active cysteine present on the surface of HSP 90 can reduce level, indicating the crucial role of HSP 90 in regulating cellular redox balance.[30] Nanozymes can leverage the enhanced permeability and retention effect exerted by solid tumours to target tumour sites. Additionally, they initiate catalytic reactions in response to the weak acidity, low oxygen levels and high H_2O_2 concentration in the tumour microenvironment.[5,14,31] Consequently, nanozymes consume endogenous substances such as glutathione (GSH) or catalyse H_2O_2 to produce highly toxic ·OH, which disrupts the redox steady state and ultimately inhibits HSPs expression. Furthermore, inorganic nanozyme has more stable structure, cost-effective preparation and preservation processes, versatile functionality, adjustable catalytic activity and better biocompatibility and safety than natural enzymes.[32] Consequently, they can be used along with PTT to achieve superior therapeutic effects.

Currently, the traditional nanomaterial-based delivery systems have poor biocompatibility. After entering the body, drugs and carriers are easily captured and removed in the process of blood circulation by the reticular endothelial system, which comprises mononuclear macrophages in systemic circulation. This results in a short blood circulation time that considerably hampers their effectiveness. In addition, as nanomaterials lack active targeting abilities, they are widely distributed throughout the body can easily cause systemic toxicity.,[33] Platelets are important circulating cells in the body that have been widely used in constructing bionic drug delivery systems.[27,33,34] Platelets have many advantages over other cells. First, platelets can specifically adhere to bleeding and injury sites.[33,35,36] Second, platelet membranes (PMs) can produce a “do not eat me” signal through the CD47 receptor on their surface, thus evading elimination by phagocytes.[37] Due to the expression of specific tumour-related receptors and proteins, PM-coated nanomaterials can accurately target tumour cells. P-selectin on the surface of PMs can recognise the CD44 receptor on the surface of tumour cells, enabling platelets to target various tumour cell lines.[38,39]

Here, we designed PM-coated CuP nanoparticles (named PC) that can be selectively delivered to the tumour site to overcome the heat resistance of tumour cells to achieve efficient and mild PTT (Scheme 1). To reliably synthesise CuP,

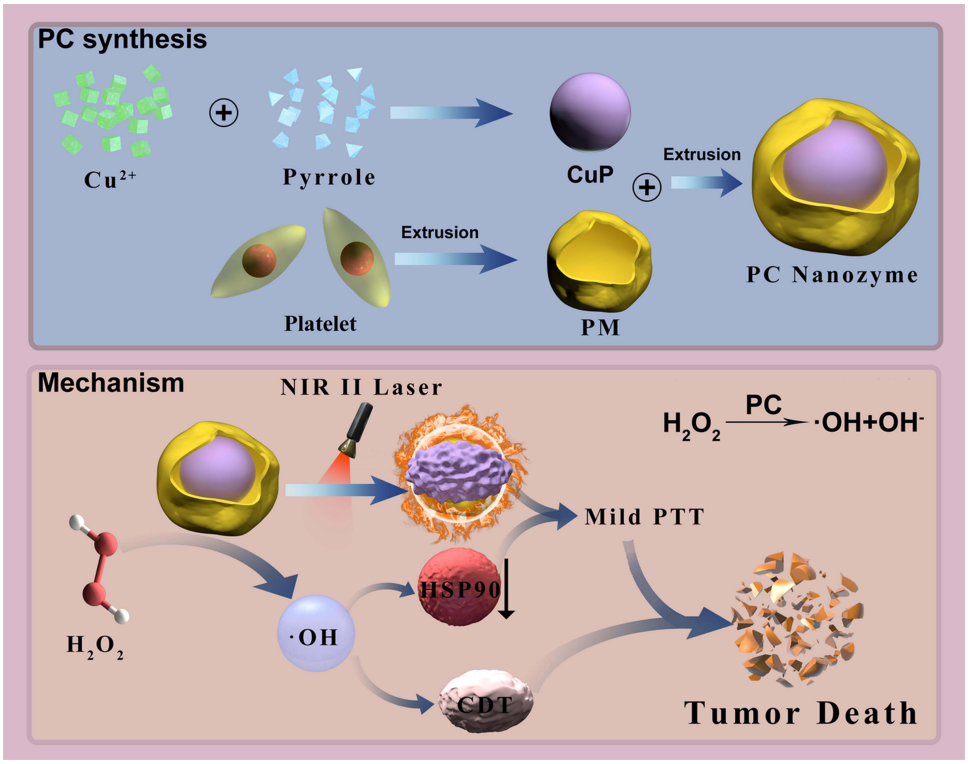

Scheme 1 Schematic illustration of biomimetic Cu-doped polypyrrole nanoparticles for enhanced cancer low-temperature PTT.

$CuCl_2$ was used as an oxidation catalyst. Polyvinyl alcohol (PVA) was used as a stabiliser during the growth of polypyrrole to achieve reliable synthesis of CuP. CuP converts light energy into heat energy in response to near-infrared II (NIR-II) laser irradiation and catalyses high level of H_2O_2 in the tumour microenvironment to produce highly toxic ·OH that kills tumour cells. In addition, PM coating increases the circulation time of PC nanoparticles in vivo and their accumulation at tumour sites. More importantly, CuP with peroxidase-like activity inhibits HSP 90 expression, thus reducing the heat resistance of cells, overcoming the photothermal resistance of tumour cells and greatly enhancing the effect of CuP-mediated mild PTT. Both in vivo and in vitro results showed that PC in conjunction with the NIR-II laser achieves a favourable tumour-killing effect and has a good biological safety. The tumour-targeted mild PTT in the NIR-II region provides more opportunities for the successful clinical application of PTT.

Results and Discussion

Preparation and Characterization of CuP Nanozymes

We synthesised CuP nanozymes from pyrrole, $CuCl_2$ and PVA.[40] The transmission electron microscopy (TEM) image shown in Figure 1A showed the structure of spherical CuP, and the image in Figure 1B showed the PM-coated CuP (PC). A membrane coating was observed on the surface of CuP, confirming the successful coating of PM. Elemental EDS-

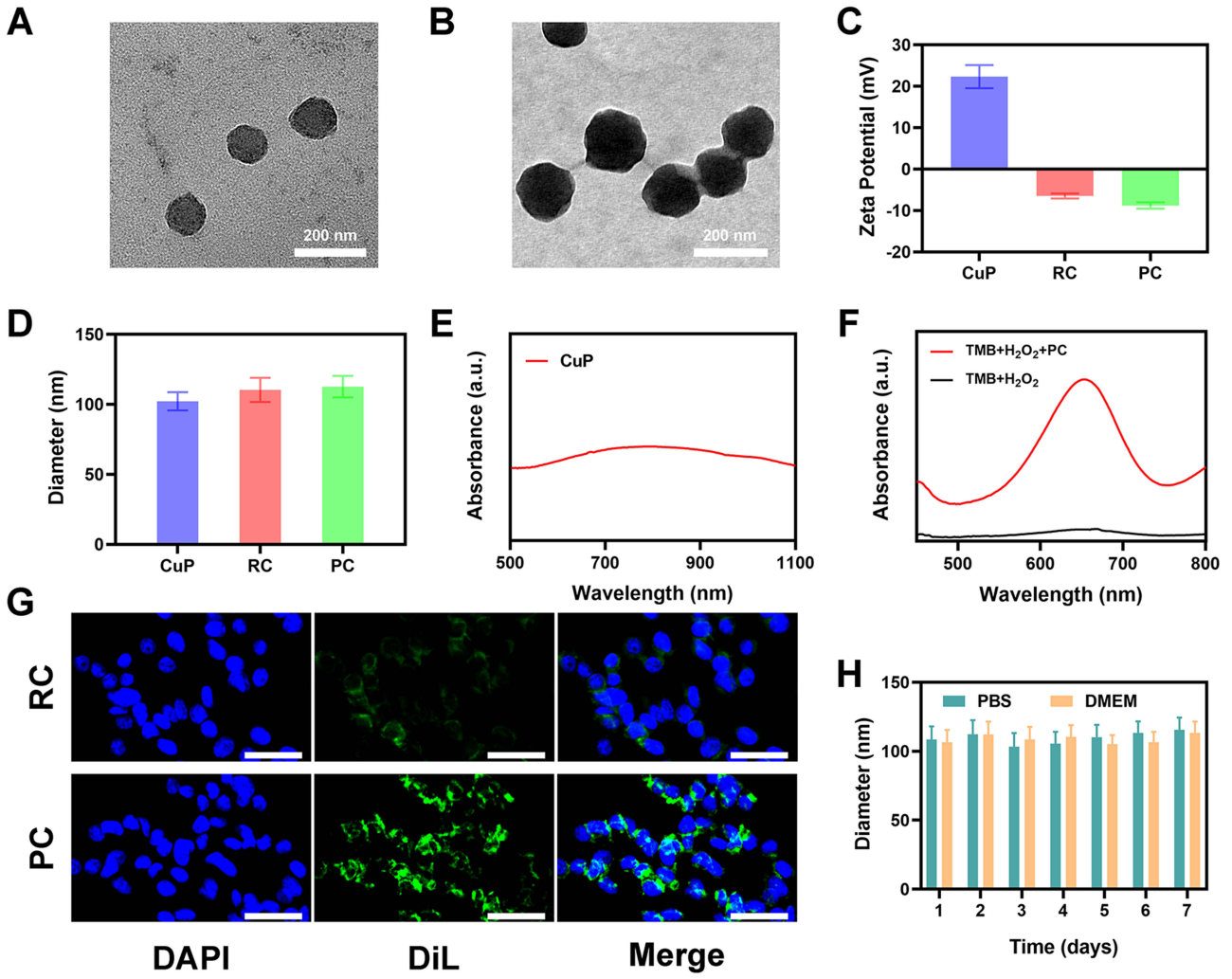

Figure 1 Characterisation of PC. (**A**) TEM image of CuP. (**B**) TEM image of PC nanozymes. (**C**) Zeta potential of CuP, RC and PC. Software: GraphPad Prism 6. (**D**) Hydrodynamic diameter of CuP, RC and PC. Software: GraphPad Prism 6. (**E**) Absorbance spectra of CuP. Software: GraphPad Prism 6. (**F**) UV/vis absorbance spectra and colour changes of TMB in different reaction systems. Software: GraphPad Prism 6. (**G**) Targeting ability of RC and PC for cancer cells. Blue: CT26 cell nucleus; green: DiL-labelled RC or PC. Scale Bar: 50 μm. (**H**) Hydrodynamic diameter changes in PC dispersed in different physiological media at different time points. Software: GraphPad Prism 6.

mapping images of PC was shown in Figure S1. The FTIR results was shown in Figure S2. The peaks located in the range of 1710–1750 cm-1 may be related to the amide bonds of proteins, while the peaks located in the range of 2920–2850 cm-1 may be related to the methyl and methylene bonds of phospholipids. The peak located near 1540–1550 cm-1 is related to the amide bond vibration of the protein. We measured the zeta potential of CuP before and after PM coating and compared both values with CuP loaded on the red cell membrane (RC), which lacked active targeting ability. The results showed that the surface zeta potential of CuP changed from 20 mV to −6 mV after co-extrusion with the erythrocyte membrane, and the zeta potential of PC also considerably decreased (Figure 1C). In addition, the particle size was measured using dynamic light scattering (Figure 1D). The sizes of RC and PC were slightly larger than that of CuP. We measured the particle size of PC incubated in different physiological media (PBS and DMEM) for a week, and the results showed that PC had good stability (Figure 1H). Cu^{2+} release from PC under different H_2O_2 condition was shown in Figure S3. The results indicated that copper ions can be slowly released from PC under the presence of hydrogen peroxide. Currently, most photothermal treatments focus on the first NIR (NIR-I) biowindow (750–1000 nm). However, the second NIR (NIR-II) biowindow (1000–1350 nm) has the advantages of having a larger maximum permissible exposure and deeper laser penetration than those of NIR-I. The UV/vis-NIR absorption spectrum showed that CuP had a broad absorption band at 1000–1100 nm, indicating its suitability for its use as NIR-II PTA (Figure 1E). Photothermal stability is a crucial aspect to assess PTAs. To further study the photothermal characteristics of PC, it was irradiated with a 1064-nm laser (0.5 W/cm^2) and the temperature curve was observed. The temperature of PC increased by approximately 24°C in 5 min. Next, the laser was turned off to allow the recovery of the initial temperature. This cycle was repeated thrice (Figure S4). The photothermal effect of PC exhibits concentration dependence (Figure S5). The results confirmed the stable photothermal performance of the PC. Using TMB as a chromogenic substrate, absorption curves of different treatment groups were measured to verify the POD activity of PC. As shown in Figure 1F, almost no peak change was observed after TMB was incubated with H_2O_2. However, a characteristic peak was produced at 652 nm after PC was added, indicating that PC can catalyse H_2O_2 to produce ·OH. Although the coating of erythrocyte membrane can prolong the circulation time of nanomaterials, it lacks targeting ability. In addition, studies have shown that copper ions can also generate hydroxyl radicals through the Fenton reaction.[40,41] The free radicals generated by PC may partially come from the released copper ions. To verify the active targeting ability of PC, DiL-labelled PC and RC were incubated with CT26 cells. Confocal laser scanning microscopy (CLSM) results showed a small number of RC entered the cells, whereas the PC group showed bright fluorescence, indicating its active targeting ability (Figure 1G). Thus, the suitability of PC as an ideal platform for actively targeted tumour cells was further validated by these experimental data.

In vitro Anti-Tumor Study

To further confirm ·OH production at the cellular level, we used DCFH-DA as a fluorescent probe to detect intracellular ·OH levels in different treatment groups using CLSM imaging (Figure 2A and C). The combination of PC with low-power NIR-II laser irradiation (PC+NIR) produced the strongest green fluorescence among all groups. This result showed that the photothermal conversion caused by PC under 1064-nm laser irradiation can greatly promote the production of ·OH radicals. The quantitative results of ROS were consistent with those of fluorescence intensity. We used an FITC-PI apoptosis kit to study the apoptosis of CT26 cells in different treatment groups (Figure 2B). Compared with the PBS group, apoptosis was not observed in the NIR group, indicating that low-power laser treatment alone had a limited effect on cell killing. The PC group achieved a certain degree of cell killing, whereas the RC+NIR group moderately inhibited cell viability, with approximately 60.3% cell viability. Notably, the PC+NIR group achieved the highest degree of apoptosis among all groups, where 31.57% and 37.44% of cells were in the early and late apoptosis stages, respectively. These results showed that the cytotoxicity of PC and NIR alone was weak, while PC+NIR achieved the effect of $1 + 1 > 2$. HSPs expression (HSP 90) was detected using Western blot analysis to verify the relationship between intracellular ROS and mild PTT. The bands shown in Figure 2D showed the expression level of HSP 90 in the different treatment groups. At 43°C, the expression of HSP 90 in cells was considerably high in all cells, but its expression was low in PC-treated cells. This observation confirmed that PC can reduce the heat tolerance of tumour cells and promote apoptosis. Furthermore, the cell counting kit-8 was used to detect cell viability in the treatment groups to study the photothermal anti-tumour effect of PC combined with the 1064-nm laser (0.5 W/cm^2) in vitro (Figure 2E and F). Consistent with the

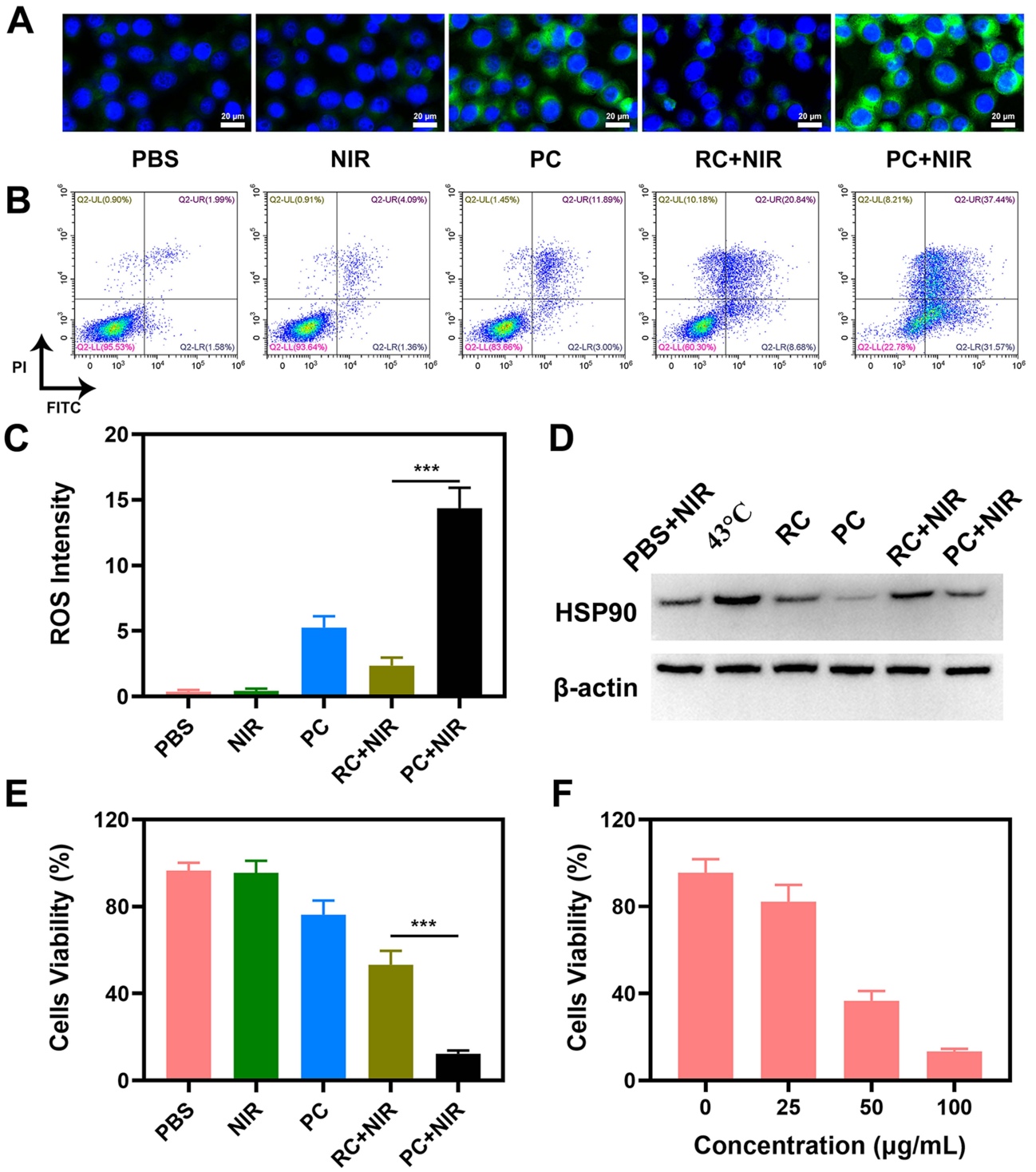

Figure 2 The PC showed synergistic anti-tumour ability in the in vitro experiments. (**A**) Confocal images of DCFH-DA in CT26 cells after treatment with different formulations. (**B**) Representative flow cytometry plots after the annexin V-FITC/PI staining of CT26 cells. (**C**) ROS fluorescence intensity after the indicated treatments. (**D**) Western blot analysis of HSP 90 after the indicated treatments. (**E**) Cell viability of CT26 cells cultured in the presence of various formulations. (**F**) Cell viability of CT26 cells cultured in the presence of PC+NIR (PC concentration: 0, 25, 50 and 100 μg/mL). Significant differences among groups as calculated using the Student's *t*-test. ***p < 0.005. Software of Figure 2C–F: GraphPad Prism 6.

previous results, the PC+NIR group showed the best cell viability inhibition effect among all groups. Notably, the PC +NIR group exhibited significant differences in cell viability compared with the RC+NIR group. This disparity may be attributed to the fact that PM coating allowed more CuP nanozymes to be phagocytised by tumour cells. Consequently, CuP catalysed intracellular H_2O_2 to produce a large number of ROS, thereby disrupting redox homeostasis, inhibiting

HSPs activity and enhancing the effectiveness of PTT. After irradiation, the cell viability of the PC treatment group showed a decreasing trend with increasing PC concentration. Overall, the in vitro cell experiments showed that our designed PC nanozyme can achieve improved tumour cell–killing ability when used in combination with NIR-II laser irradiation.

In vivo Anti-Tumor Study

The prerequisite for effectively treating tumours using nanomaterials is having the ability to achieve high enrichment efficiency in tumour sites. Considering that the tumour cell membrane can improve the cell uptake and targeting efficiency of PC in vitro, we initially studied the uptake ability of PC and RC in subcutaneous tumours of CT26 tumour-bearing mice. Pharmacokinetic experiments showed that both PC and RC groups achieved good long-term circulation (Figure 3A). An in vivo biological distribution experiment showed that RC and PC mainly accumulated in the liver. However, RC exhibited lower accumulation at the tumour site than PC, confirming the active targeting ability of PM in vivo (Figure 3B). In platelets, the CD44 protein targeted tumour cells through the P-selectin protein on the surface. As a critical PM protein, P-selectin plays an important role in tumour targeting.[34,35,42]

Photothermal imaging technology was used to evaluate the photothermal conversion performance of PC in vivo. After injecting different formulations into CT26 tumour-bearing mice through the tail vein for 12 hours, the temperature

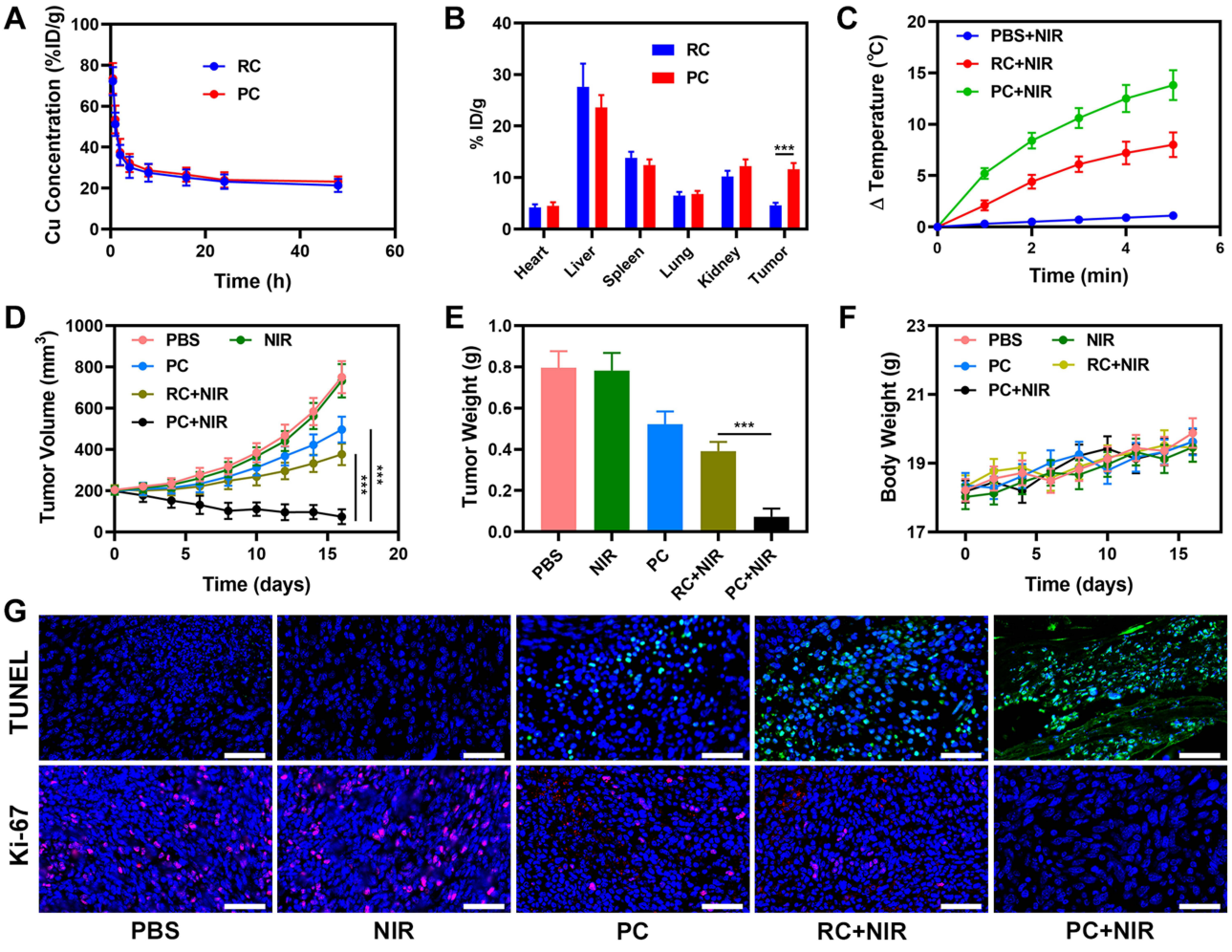

Figure 3 In vivo anti-tumour capability analysis. (**A**) Pharmacokinetic behaviour of RC and PC. (**B**) Quantitative analysis of Cu biodistribution in tissues and tumours of tumour-bearing mice injected with RC and PC. (**C**) Temperature change of the tumour upon laser irradiation. (**D**) Relative changes in tumour volume in mice after the indicated treatments. (**E**) Evolution of the tumour weight during therapy. (**F**) Changes in the body weight of the mice recorded every other day after the indicated treatments. (**G**) TUNEL and Ki-67 staining of tumour sections from the tumour-bearing mice. Scale bars:50μm. Significant differences among the groups as calculated using the Student's *t*-test. ***p < 0.005. Software of Figure 3A–F: GraphPad Prism 6.

change at the tumour site was recorded using an infrared thermal imager under 1064-nm laser irradiation. The temperature of the PBS+NIR group barely increased over time, while that of the PC+NIR group increased significantly, rising by approximately 13.8°C within 5 min (Figure 3C), indicating the considerable potential for achieving a PTT effect in tumour treatment. Next, we investigated the anti-tumour effect of PC-mediated PTT in vivo. The CT26 tumour-bearing mice were randomly divided into five groups: (1) PBS, (2) NIR, (3) PC, (4) RC+NIR and (5) PC+NIR. The tumour size and body weight of the mice were measured every 2 days after administering different treatments.

The tumour volume increased rapidly in the PBS and NIR groups; however, the tumour volume in the PC group showed slight growth stagnation (Figure 3D). The tumour volume of the RC+NIR group gradually increased in the first week and then slowly increased in the following week, indicating a moderate treatment effect. Notably, the tumour volume curve of the PC+NIR group decreased steadily over time, suggesting that the PC nanozyme achieved efficient mild PTT, thus inhibiting tumour growth. After the treatment, tumour tissues of each group were imaged and weighed and the average weight of tumour tissues was compared across different treatment groups (Figures S6 and S7). As shown in Figure 3E, the tumour weight of the PC+NIR group significantly differed from that of the other groups, which confirmed that PC+NIR group had a stronger tumour inhibition effect. Furthermore, we monitored changes in the weight of mice in the different treatment groups. During the treatment, the weight of mice in each group did not change considerably but increased slowly, indicating that our treatment method had no obvious toxicity in vivo (Figure 3F).

To further study the mechanism underlying tumour tissue destruction in the CH+NIR group, we stained the tumour tissue to detect proliferation and apoptosis signals after the treatment (Figure 3G). TUNEL staining showed that the PC +NIR group induced the best apoptosis among all groups. The image of tissues stained with Ki-67, an antigen related to cell proliferation, showed that the expression of Ki67 protein in the PC+NIR group was remarkably reduced. This result proves that combining PC and NIR can enhance cancer treatment.

Biosafety Assessment

In addition, we conducted further tests to evaluate the impact of PC on the blood biochemical indexes of the PC+NIR group. Figure 4A–E showed that the indexes of mice were within the normal range, confirming that the safety of the treatment. After the treatment, main organs (heart, liver, spleen, lung and kidney) of the mice were stained with hematoxylin and eosin (H&E). Histological analysis of H&E staining results showed no obvious pathological changes

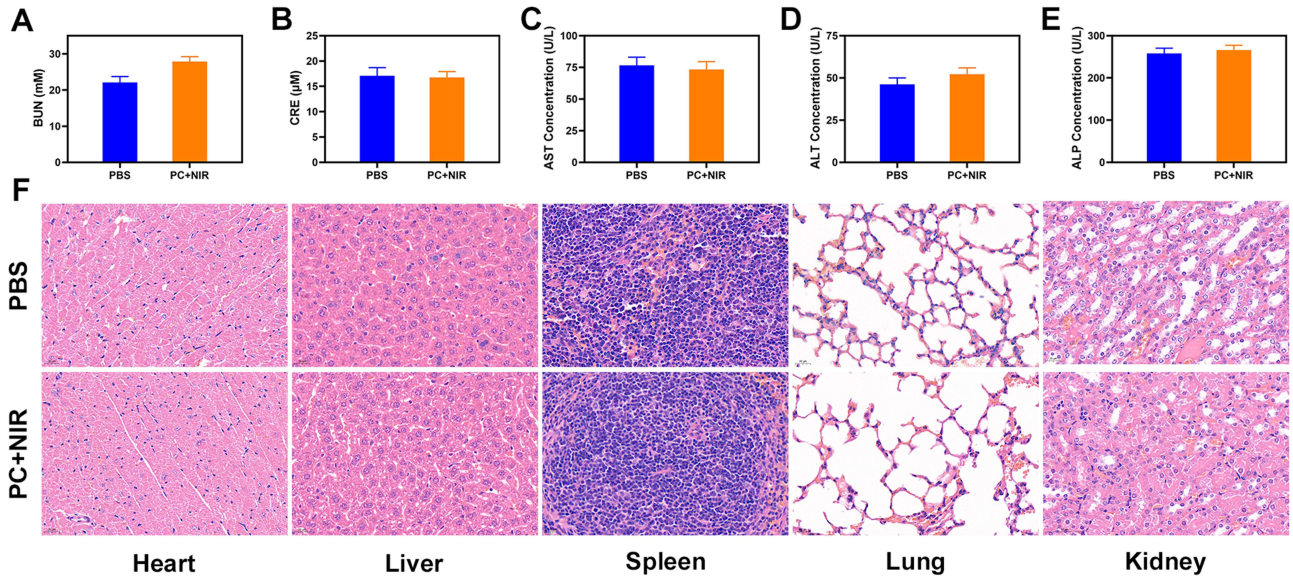

Figure 4 Result of in vivo safety experiments. (**A–E**) Blood biochemistry data showed kidney and liver function markers (BUN, CRE, AST, ALT and ALP) after various treatments. (**F**) Histopathological analysis results from H&E-stained images of major organs, including heart, lung, liver, kidneys and spleen of mice, which were exposed to different treatments 16 days post-injection under laser irradiation. Software of Figure 4A–E: GraphPad Prism 6.

in the PC group, even under NIR laser irradiation (Figure 4F), which indicated that the biological safety of PC in vivo was acceptable.

Conclusions

In this study, a biomimetic nanozyme system (termed "PC") was designed to enable the administration of mild PTT. PM coating significantly prolonged the blood circulation time of PC while enabling PC to achieve tumour targeting. PC, which possessed POD activity, catalysed intracellular H_2O_2 to generate abundant ·OH and consequently induce tumour cell death. Additionally, this process inhibited the expression of HSP 90, thereby reducing the thermal tolerance of tumour tissues and enhancing the effectiveness of mild PTT under the irradiation of a 1064-nm laser with low power density. In addition, this treatment approach showed good biological safety, with no noticeable abnormalities in any of the treatment groups. Thus, this system can be used as a novel strategy for enhancing mild photothermal tumour therapy.

Acknowledgments

We are grateful for the financial support from the Outstanding Youths Development Scheme of Nanfang Hospital, Southern Medical University (2021J008), the National Natural Science Foundation of China (grant number: 82202461), Hubei Provincial Natural Science Foundation of China (2021CFB043, ZRMS2022000981), the Science and Technology Projects in Guangzhou (2023A04J2370), and Hubei Province key research and development project (2023BCB088). We thank Dr. He Guijuan for her assistance and support in this work.

Disclosure

The authors report no conflicts of interest in this work.

References

1. Yu H, Guo H, Zu H, et al. Therapeutic dendritic cell vaccines engineered with antigen-biomineralized Bi2S3 nanoparticles for personalized tumor radioimmunotherapy. *Aggregate*. 2022;3:e194. doi:10.1002/agt2.194
2. Sun J, He X. AIE-based drug/gene delivery system: evolution from fluorescence monitoring alone to augmented therapeutics. *Aggregate*. 2022;3:e282.
3. Zhu D, Lyu M, Huang Q, et al. Stellate plasmonic exosomes for penetrative targeting tumor NIR-II thermo-radiotherapy. *ACS Appl Mater Interfaces*. 2020;12:36928–36937. doi:10.1021/acsami.0c09969
4. Zhu D, Zheng Z, Luo G, et al. Single injection and multiple treatments: an injectable nanozyme hydrogel as AIEgen reservoir and release controller for efficient tumor therapy. *Nano Today*. 2021;37:101091.
5. Zhang T, Liu Z, Tang W, et al. Mitochondria-targeting Type I AIE photosensitizer combined with H2S therapy: uninterrupted hydroxyl radical generation for enhancing tumor therapy. *Nano Today*. 2022;46:101620. doi:10.1016/j.nantod.2022.101620
6. Cheng L, He W, Gong H, et al. PEGylated micelle nanoparticles encapsulating a non-fluorescent near-infrared organic dye as a safe and highly-effective photothermal agent for in vivo cancer therapy. *Adv Funct Mater*. 2013;23:5893–5902. doi:10.1002/adfm.201301045
7. Li X, Kong L, Hu W, et al. Safe and efficient 2D molybdenum disulfide platform for cooperative imaging-guided photothermal-selective chemotherapy: a preclinical study. *J Adv Res*. 2021;37:255–66.
8. Li X, Xing L, Zheng K, Wei P, Du L. Formation of gold nanostar-coated hollow mesoporous silica for tumor multimodality imaging and photothermal therapy. *ACS Appl Mater Interfaces*. 2017;9:5817–5827. doi:10.1021/acsami.6b15185
9. Yang Y, Zhu W, Dong Z, et al. 1D coordination polymer nanofibers for low-temperature photothermal therapy. *Adv Mater*. 2017;29. doi:10.1002/adma.201703588
10. Ding F, Gao X, Huang X, et al. Polydopamine-coated nucleic acid nanogel for siRNA-mediated low-temperature photothermal therapy. *Biomaterials*. 2020;245:119976. doi:10.1016/j.biomaterials.2020.119976
11. Chen QW, Liu XH, Fan JX, et al. Self-mineralized photothermal bacteria hybridizing with mitochondria-targeted metal–organic frameworks for augmenting photothermal tumor therapy. *Adv Funct Mater*. 2020;1909806. doi:10.1002/adfm.201909806
12. Wu J, Ning P, Gao R, et al. Programmable ROS-mediated cancer therapy via magneto-inductions. *Adv Sci*. 2020;1902933. doi:10.1002/advs.201902933
13. Zhang X, Ong'achwa Machuki J, Pan W, et al. Carbon nitride hollow theranostic nanoregulators executing laser-activatable water splitting for enhanced ultrasound/fluorescence imaging and cooperative phototherapy. *ACS nano*. 2020;14:4045–4060. doi:10.1021/acsnano.9b08737
14. Zhu D, Chen H, Huang C, et al. H_2O_2 self-producing single-atom nanozyme hydrogels as light-controlled oxidative stress amplifier for enhanced synergistic therapy by transforming "cold" tumors. *Adv Funct Mater*. 2022;32:2110268. doi:10.1002/adfm.202110268
15. Ning S, Lyu M, Zhu D, et al. Type-I AIE photosensitizer loaded biomimetic system boosting cuproptosis to inhibit breast cancer metastasis and rechallenge. *ACS nano*. 2023. doi:10.1021/acsnano.3c00326
16. Zhang T, Zhang J, Wang FB, et al. Mitochondria-targeting phototheranostics by aggregation-induced NIR-II emission luminogens: modulating intramolecular motion by electron acceptor engineering for multi-modal synergistic therapy. *Adv Funct Mater*. 2022;2110526. doi:10.1002/adfm.202110526
17. Zhu D, Zhang J, Luo G, Duo Y, Tang BZ. Bright bacterium for hypoxia-tolerant photodynamic therapy against orthotopic colon tumors by an interventional method. *Adv Sci*. 2021;8:2004769. doi:10.1002/advs.202004769

18. Zhu D, Duo Y, Meng S, et al. Tumor-exocytosed exosome/aggregation-induced emission luminogen hybrid nanovesicles facilitate efficient tumor penetration and photodynamic therapy. *Angew Chem*. 2020;59:2–10.
19. Duo Y, Zhu D, Sun X, et al. Patient-derived microvesicles/AIE luminogen hybrid system for personalized sonodynamic cancer therapy in patient-derived xenograft models. *Biomaterials*. 2021;272:120755. doi:10.1016/j.biomaterials.2021.120755
20. Zhu D, Zhang T, Li Y, et al. Tumor-derived exosomes co-delivering aggregation-induced emission luminogens and proton pump inhibitors for tumor glutamine starvation therapy and enhanced type-I photodynamic therapy. *Biomaterials*. 2022;283:121462. doi:10.1016/j.biomaterials.2022.121462
21. Wang K, Li Y, Wang X, et al. Gas therapy potentiates aggregation-induced emission luminogen-based photoimmunotherapy of poorly immunogenic tumors through cGAS-STING pathway activation. *Nat Commun*. 2023;14:2950. doi:10.1038/s41467-023-38601-7
22. Kankala RK, Liu C-G, Chen A-Z, et al. Overcoming multidrug resistance through the synergistic effects of hierarchical pH-sensitive, ROS-generating nanoreactors. *ACS Biomater Sci Eng*. 2017;3:2431–2442. doi:10.1021/acsbiomaterials.7b00569
23. Kankala RK, Tsai P-Y, Kuthati Y, Wei P-R, Liu C-L, Lee C-H. Overcoming multidrug resistance through co-delivery of ROS-generating nano-machinery in cancer therapeutics. *J Mater Chem B*. 2017;5:1507–1517. doi:10.1039/C6TB03146C
24. Han Y-H, Liu C-G, Chen B-Q, et al. Orchestrated tumor apoptosis (Cu2+) and bone tissue calcification (Ca2+) by hierarchical Copper/Calcium-ensembled bioactive silica for osteosarcoma therapy. *Chem Eng J*. 2022;435:134820. doi:10.1016/j.cej.2022.134820
25. Chen B-Q, Zhao Y, Zhang Y, et al. Immune-regulating camouflaged nanoplatforms: a promising strategy to improve cancer nano-immunotherapy. *Bioact Mater*. 2023;21:1–19. doi:10.1016/j.bioactmat.2022.07.023
26. Liu C-G, Han Y-H, Zhang J-T, Kankala RK, Wang S-B, Chen A-Z. Rerouting engineered metal-dependent shapes of mesoporous silica nanocontainers to biodegradable Janus-type (sphero-ellipsoid) nanoreactors for chemodynamic therapy. *Chem Eng J*. 2019;370:1188–1199. doi:10.1016/j.cej.2019.03.272
27. Ning S, Zhang T, Lyu M, et al. A type I AIE photosensitiser-loaded biomimetic nanosystem allowing precise depletion of cancer stem cells and prevention of cancer recurrence after radiotherapy. *Biomaterials*. 2023;295. doi:10.1016/j.biomaterials.2023.122034
28. Zhu D, Liu Z, Li Y, Huang Q, Xia L, Li K. Delivery of manganese carbonyl to the tumor microenvironment using tumor-derived exosomes for cancer gas therapy and low dose radiotherapy. *Biomaterials*. 2021;274:120894. doi:10.1016/j.biomaterials.2021.120894
29. Choi YJ, Om JY, Kim NH, et al. Heat shock transcription factor-1 suppresses apoptotic cell death and ROS generation in 3-nitropropionic acid-stimulated striatal cells. *Mol Cell Biochem*. 2013;375:59–67.
30. Gallerne C, Prola A, Lemaire C. Hsp90 inhibition by PU-H71 induces apoptosis through endoplasmic reticulum stress and mitochondrial pathway in cancer cells and overcomes the resistance conferred by Bcl-2. *BBA*. 2013;1833:1356–1366. doi:10.1016/j.bbamcr.2013.02.014
31. Wang C, Wu J, Wang Z, et al. Glutamine addiction activates polyglutamine-based nanocarriers delivering therapeutic siRNAs to orthotopic lung tumor mediated by glutamine transporter SLC1A5. *Biomaterials*. 2018;183:77–92. doi:10.1016/j.biomaterials.2018.08.035
32. Tang G, He J, Liu J, Yan X, Fan K. Nanozyme for tumor therapy: surface modification matters. *Exploration*. 2021;1:75–89. doi:10.1002/EXP.20210005
33. Chen T, Luo X, Zhu L, et al. Biomimetic single-atom nanozyme system for efficient inhibition of gastric cancer ascites via SO2 gas-enhanced nanocatalytic cancer therapy. *Chem Eng J*. 2023;467. doi:10.1016/j.cej.2023.143386
34. Zhu D, Ling R, Chen H, et al. Biomimetic copper single-atom nanozyme system for self-enhanced nanocatalytic tumor therapy. *Nano Res*. 2022;15:7320–7328. doi:10.1007/s12274-022-4359-6
35. Lyu M, Chen M, Liu L, et al. A platelet-mimicking theranostic platform for cancer interstitial brachytherapy. *Theranostics*. 2021;11:7589–7599. doi:10.7150/thno.61259
36. Chen H, Luo X, Huang Q, et al. Platelet membrane fusion liposome loaded with type I AIE photosensitizer to induce chemoresistance cancer pyroptosis and immunogenic cell death for enhancing cancer immunotherapy. *Chem Eng J*. 2023;476. doi:10.1016/j.cej.2023.146276
37. Fang RH, Kroll AV, Gao W, Zhang L. Cell membrane coating nanotechnology. *Adv Mater*. 2018;30:e1706759. doi:10.1002/adma.201706759
38. Chen Y, Zhao G, Wang S, et al. Platelet-membrane-camouflaged bismuth sulfide nanorods for synergistic radio-photothermal therapy against cancer. *Biomater Sci*. 2019;7:3450–3459. doi:10.1039/C9BM00599D
39. Ye H, Wang K, Wang M, et al. Bioinspired nanoplatelets for chemo-photothermal therapy of breast cancer metastasis inhibition. *Biomaterials*. 2019;206:1–12. doi:10.1016/j.biomaterials.2019.03.024
40. Chen T, Zeng W, Liu Y, et al. Cu-doped polypyrrole with multi-catalytic activities for sono-enhanced nanocatalytic tumor therapy. *Small*. 2022;18:e2202964. doi:10.1002/smll.202202964
41. Zheng -N-N, Kong W-Y, Huang Z, et al. Novel theranostic nanoagent based on CuMo2S3-PEG-Gd for MRI-guided photothermal/photodynamic/chemodynamic therapy. *Rare Metals*. 2022;41:45–55. doi:10.1007/s12598-021-01793-2
42. Yang M-Y, Tu Y-F, Feng -K-K, et al. A erythrocyte-platelet hybrid membrane coated biomimetic nanosystem based on ginsenosides and PFH combined with ultrasound for targeted delivery in thrombus therapy. *Colloids Surf B*. 2023. doi:10.1016/j.colsurfb.2023.113468